Nematic ordering in the Heisenberg spin-glass system in three dimensions

Egemen Tunca[1] and A. Nihat Berker[2,3,4]

[1]*TEBIP High Performers Program, Board of Higher Education of Turkey, Istanbul University, Fatih, Istanbul 34452, Turkey*

[2]*Faculty of Engineering and Natural Sciences, Kadir Has University, Cibali, Istanbul 34083, Turkey*

[3]*TÜBITAK Research Institute for Fundamental Sciences, Gebze, Kocaeli 41470, Turkey*

[4]*Department of Physics, Massachusetts Institute of Technology, Cambridge, Massachusetts 02139, USA*

(Received 4 August 2022; revised 1 December 2022; accepted 23 December 2022; published 13 January 2023)

Nematic ordering, where the spins globally align along a spontaneously chosen axis irrespective of direction, occurs in spin-glass systems of classical Heisenberg spins in $d = 3$. In this system where the nearest-neighbor interactions are quenched randomly ferromagnetic or antiferromagnetic, instead of the locally randomly ordered spin-glass phase, the system orders globally as a nematic phase. This nematic ordering of the Heisenberg spin-glass system is dramatically different from the spin-glass ordering of the Ising spin-glass system. The system is solved exactly on a hierarchical lattice and, equivalently, Migdal-Kadanoff approximately on a cubic lattice. The global phase diagram is calculated, exhibiting this nematic phase, and ferromagnetic, antiferromagnetic, disordered phases. The nematic phase of the classical Heisenberg spin-glass system is also found in other dimensions $d > 2$: We calculate nematic transition temperatures in 24 different dimensions in $2 < d \leqslant 4$.

DOI: 10.1103/PhysRevE.107.014116

I. INTRODUCTION: NEMATIC ORDER DUE TO QUENCHED RANDOMNESS

Spin glasses [1–8], broadly defined as systems with frozen (quenched) disorder that have locally annulling interactions (frustration), present complex systems with a plethora of distinctive characteristics. These distinctions include the spin-glass phase and its signature: chaos under repeated scale changes [9–11]. The fractal spectrum of spin-glass chaos has recently been shown to be used as a classification and clustering tool for the broadest of complex data, including multigeographic multicultural music and brain signals [12]. The ordering of the spin-glass phase has local fixation within spatial nonuniformity, the direction and magnitude of the local magnetization varying between neighboring points of a lattice, but the direction of local magnetization being firmly fixed relative to the local magnetizations of the neighbors.

The above discussion has been in terms of Ising spins, namely one-component spins, on which the preponderance of spin-glass research has been done. We find here that for three-component Heisenberg spins [7,8,13–22], the new ordering evades the directional fixation: The spins globally align along a spontaneously chosen axis irrespective of direction, thus creating a nematic spin phase. Thus, symmetry is globally broken by the spontaneous choice of a spin axis, but all local magnetizations are zero.

In previous research on the $d = 3$ classical Heisenberg spin-glass systems [7,8,13–22], the existence of a phase transition has been established by Monte Carlo simulation, but without our nematic-order characterization. However, as explained below, the existence of a narrow intermediate chiral spin-glass phase is controversial. We definitely find a low-temperature phase of nematic order, dramatically different from Ising spin-glass order as explained below, in 24 different spatial dimensions that we calculated in $2.26 \leqslant d \leqslant 4$, including $d = 3$, and no intermediate chiral spin-glass phase. We find no ordered phase in $d = 2$, as expected since the pure Heisenberg ferromagnet or antiferromagnet itself does not order in $d = 2$ [23].

II. MODEL AND GENERAL METHOD

The classical Heisenberg spin-glass system is defined by the Hamiltonian

$$-\beta\mathcal{H} = \sum_{\langle ij \rangle} J_{ij}\, \vec{s}_i \cdot \vec{s}_j, \tag{1}$$

where $\beta = 1/k_B T$, $J_{ij} = +|J|$ or $-|J|$ (ferromagnetic or antiferromagnetic) with probability $1 - p$ and p, respectively, the classical spin $\vec{s}_i$ is the unit spherical vector at lattice site i, and the sum is over all nearest-neighbor pairs of sites.

We solve the classical Heisenberg spin glass by a renormalization-group transformation that is exact on the $d = 3$ hierarchical lattice (Fig. 1) and, equivalently, Migdal-Kadanoff approximate [28,29] on the $d = 3$ cubic lattice. The latter much-used approximation is physically intuitive: In a hypercubic lattice where an exact renormalization-group transformation cannot be applied, as an approximation some of the bonds are removed, which weakens the connectivity of the system and, to compensate, for every bond removed, a bond is added to the remaining bonds (before or after the decimation, in two different versions of the procedure [29]). This step is the bond-moving step and constitutes the approximate step of the renormalization-group transformation. At this point, the intermediate sites can be eliminated by an exact integration over their spin values in

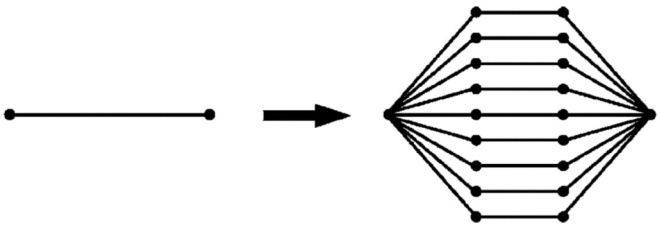

FIG. 1. Construction of the $d = 3$ hierarchical model used in this study. A hierarchical model is constructed by repeatedly self-imbedding a graph into each of its bonds. This hierarchical model is the $d = 3, b = 3$ generalization of the original $d = 2, b = 2$ hierarchical model introduced in Fig. 2(c) of Ref. [24] in 1979 and is a member of the most used family of hierarchical models, namely the so-called "diamond" family. For example, this model family has been used [25] in the determination of the spin-glass lower-critical dimension by solving in 23 sequenced dimensions d. The exact solution of a hierarchical model proceeds in the opposite direction of its construction [24,26,27].

the partition function, which yields the interaction between the remaining sites. This is called the (exact) decimation step and completes the renormalization-group transformation. In any case, the renormalization-group recursion relations of the Migdal-Kadanoff approximation are identical to those of an exact solution of a hierarchical model [24,26,27]. That the Migdal-Kadanoff renormalization-group calculation is the exact solution on a d-dimensional hierarchical lattice [11,24,26,27] makes it a physically realizable approximation, for example used in polymers [30,31], disordered alloys [32], and turbulence [33]. For recent works directly using hierarchical models, see Refs. [34–46].

This simple, physically intuitive, and easily implemented renormalization-group transformation has been widely successful on different systems, namely on essentially the entire range of standard and complex systems in the physical dimensions: Among the early achievements were the nonadjustedly experimentally matching global phase diagrams of surface systems [47,48] starting with known microscopic potentials and later work includes the calculation of high-temperature superconductivity phase diagrams [49]. The lower-critical dimension d_c below which no ordering occurs has been correctly determined as $d_c = 1$ for the Ising model [28,29], $d_c = 2$ for the XY [50,51] and Heisenberg [23] models, and the presence of an algebraically ordered phase has been seen for the XY model [42,50,51]. In q-state Potts models, the number of states q_c for the changeover from second-order to first-order phase transitions has been correctly obtained in $d = 2$ and 3 [52]. In systems with frozen microscopic disorder (quenched randomness), $d_c = 2$ has been determined for the random-field Ising [53,54] and XY models [55], and the noninteger value of $d_c = 2.46$ for the Ising spin glass [25,56–61]. In systems with quenched bond (temperature) randomness, the changeover from first-order to second-order phase transitions, with infinitesimal randomness in $d = 2$ [62–65] and with a threshold randomness in $d > 2$ [64,65], has been calculated. The chaotic nature of the Ising spin-glass phases [9–11] has been obtained and Lyapunov exponent-wise quantitatively analyzed, both for quenched randomly mixed ferromagnetic-antiferromagnetic spin glasses [66–68] and right- and left-chiral (helical) spin glasses [69–71].

III. RENORMALIZATION-GROUP TRANSFORMATION FOR THE HEISENBERG MODEL WITH NONUNIFORM INTERACTIONS

The algebra of this renormalization-group transformation for discrete spin systems such as Ising, Potts, and clock models is quite simple. The transformation for the three-component classical Heisenberg model, with each spin having two continuously varying sterangles, has only been recently achieved [23], for systems without randomness, and is not simple. Here, we generalize this renormalization-group transformation to quenched random systems.

In the first, decimation, step of the renormalization-group transformation, a decimated bond is obtained by integrating over the shared spin of two bonds. With $u_{ij}(\gamma) = e^{-\beta \mathcal{H}_{ij}(\vec{s}_i,\vec{s}_j)}$ being the exponentiated nearest-neighbor Hamiltonian between sites (i, j) and γ_{ij} being the angle between the spherical unit vectors $(\vec{s}_i, \vec{s}_j)$, the decimation proceeds as

$$\begin{aligned}\tilde{u}_{13}(\gamma_{13}) &= \int u_{12}(\gamma_{12}) u_{23}(\gamma_{23}) \frac{d\vec{s}_2}{4\pi} \\ &= \sum_{l_1=0}^{\infty} \sum_{l_2=0}^{\infty} \int \lambda_{l_1}^{(12)} \lambda_{l_2}^{(23)} P_{l_1}(\cos\gamma_{12}) P_{l_2}(\cos\gamma_{23}) \frac{d\vec{s}_2}{4\pi},\end{aligned} \tag{2}$$

where the Fourier-Legendre series is used,

$$u_{ij}(\gamma) = \sum_{l=0}^{\infty} \lambda_l^{(ij)} P_l(\cos\gamma), \tag{3}$$

with the expansion coefficient $\lambda_l^{(ij)}$ evaluated as

$$\lambda_l^{(ij)} = \frac{2l+1}{2} \int_{-1}^{1} u_{ij}(\gamma) P_l(\cos\gamma)\, d(\cos\gamma). \tag{4}$$

Expressing the Legendre polynomials in terms of spherical harmonics,

$$\begin{aligned}\tilde{u}_{13}(\gamma_{13}) = \sum_{l_1=0}^{\infty} \sum_{l_2=0}^{\infty} \sum_{m_1=-l_1}^{l_1} \sum_{m_2=-l_2}^{l_2} \lambda_{l_1}^{(12)} \lambda_{l_2}^{(23)} \frac{(4\pi)^2}{(2l_1+1)(2l_2+1)} \\ \times \int Y_{l_1}^{m_1}(\vec{s}_1) Y_{l_1}^{m_1 *}(\vec{s}_2) Y_{l_2}^{m_2}(\vec{s}_2) Y_{l_2}^{m_2 *}(\vec{s}_3) \frac{d\vec{s}_2}{4\pi},\end{aligned} \tag{5}$$

evaluating the integral and summing over the resulting delta functions,

$$= \sum_{l_1=0}^{\infty} \sum_{m_1=-l_1}^{l_1} \lambda_{l_1}^{(12)} \lambda_{l_1}^{(23)} \frac{4\pi}{(2l_1+1)^2} Y_{l_1}^{m_1}(\vec{s}_1) Y_{l_1}^{m_1 *}(\vec{s}_3), \tag{6}$$

due to occurring Dirac delta functions. Rearranging the spherical harmonics back to Legendre polynomials, we simply obtain

$$\tilde{\lambda}_l^{(13)} = \frac{\lambda_l^{(12)} \lambda_l^{(23)}}{2l+1}. \tag{7}$$

The tilde denotes decimated. This procedure is repeated until the length-rescaling factor b is obtained, namely until b bonds in a series are replaced by one decimated bond.

In the second, bond-moving step (Fig. 1) of the renormalization-group transformation,

$$u'_{ij}(\gamma) = \tilde{u}^A_{ij}(\gamma)\tilde{u}^B_{ij}(\gamma), \tag{8}$$

where Eq. (8) combines two different (due to quenched randomness) interactions, as seen in Fig. 1, between the spins at sites (i, j). Thus, Fourier-Legendre transforming Eq. (8),

$$\begin{aligned}\lambda'_l &= \frac{2l+1}{2}\int_{-1}^{1} \tilde{u}^A(\gamma)\tilde{u}^B(\gamma)P_l(\cos\gamma)\,d(\cos\gamma) \\ &= \frac{2l+1}{2}\sum_{l_1=0}^{\infty}\sum_{l_2=0}^{\infty}\tilde{\lambda}^A_{l_1}\tilde{\lambda}^B_{l_2} \\ &\quad\times\int_{-1}^{1} P_{l_1}(\cos\gamma)P_{l_2}(\cos\gamma)P_l(\cos\gamma)d(\cos\gamma) \\ &= \sum_{l_1=0}^{\infty}\sum_{l_2=0}^{\infty}\tilde{\lambda}^A_{l_1}\tilde{\lambda}^B_{l_2}\langle l_1 l_2 00|l_1 l_2 l 0\rangle^2,\end{aligned} \tag{9}$$

where the bracket notation is the Clebsch-Gordan coefficient with the restrictions $l_1 + l_2 + l = 2s, s \in \mathbf{N}$; $|l_1 - l_2| \leqslant l \leqslant |l_1 + l_2|$. The prime denotes renormalized. This bond moving is repeated until the total of $b^{(d-1)}$ bonds are moved.

This completes the renormalization-group transformation, which is thus in terms of the Fourier-Legendre coefficients $\lambda'_l(\{\lambda_l\})$. We have kept at least $l = 21$ (and up to 49) Fourier-Legendre coefficients in our numerical calculations of the trajectories.

IV. RENORMALIZATION-GROUP TRANSFORMATION FOR THE HEISENBERG MODEL WITH QUENCHED RANDOMNESS

Having derived the renormalization-group transformation for nonuniform nearby interactions, we can now proceed with the solution of the quenched random problem of the spin-glass Heisenberg system in d dimensions, exactly on hierarchical lattices and Migdal-Kadanoff approximately on hypercubic lattices.

For the renormalization-group transformation of the quenched probability distribution [25,53–55,61,66–72], we start with a distribution comprising 30 000 local ferromagnetic and antiferromagnetic interactions as dictated by the ferromagnetic probability $1 - p$ given after Eq. (1). From this group, we randomly select b^d interactions and effect the local renormalization-group transformation described above, to generate one of the renormalized interactions. We repeat this random selection and local transformation 30 000 times, generating 30 000 renormalized interactions and hence the renormalized quenched probability distribution. Remembering that for each interaction, at least 21 Fourier-Legendre coefficients are kept, this is a gigantic calculation. In order to conserve the ferromagnetic-antiferromagnetic symmetry of the system, the length rescaling factor of $b = 3$ is chosen. In the decimation step, b interactions in series are decimated into one. In the bond-moving step, b^{d-1} interactions are moved onto one interaction.

The renormalization-group trajectories (of sets of 30 000 interactions with each interaction determined by 21 Fourier-Legendre coefficients, thus a total of 630 000 data points flowing under renormalization group) are effected by repeated applications of the above transformation. The initial points of these trajectories are obtained from the Hamiltonian in Eq. (1), which can be written as

$$-\beta\mathcal{H} = \sum_{\langle ij\rangle} J_{ij}\vec{s}_i\cdot\vec{s}_j = \sum_{\langle ij\rangle} J_{ij}\cos\gamma_{ij}. \tag{10}$$

Using the plane-wave expansion for the term in the partition function involving the two spins,

$$e^{J\cos\gamma} = \sum_{l=0}^{\infty}(2l+1)i^l j_l(-iJ)P_l(\cos\gamma) = \sum_{l=0}^{\infty}\lambda_l P_l(\cos\gamma), \tag{11}$$

where $j_l(-iJ)$ is a spherical Bessel function and $P_l(\cos\gamma)$ is a Legendre polynomial. The middle part in Eq. (11) shows the spherical Bessel functions as the initial conditions of the renormalization-group flows.

With no approximation, after every bond moving and after setting up the initial conditions, the coefficients $\{\lambda_l\}$ are divided by the largest λ_l. This is equivalent to subtracting a constant term from the Hamiltonian and prevents numerical overflow problems in flows inside the ordered phases.

V. NEMATIC PHASE: GLOBAL ALIGNMENT SPONTANEOUSLY GENERATED FROM SPIN-GLASS DISORDER

Under repeated applications of the renormalization-group transformation of Eq. (9), the Fourier-Legendre coefficients flow to a stable fixed point, which is the sink of a thermodynamic phase. The sinks of the disordered phase and the ferromagnetic phase have been discussed and analyzed elsewhere [23]. The sink of the ferromagnetic phase is a sharp central peak at the nearest-neighbor angle $\gamma = 0$. The sink of the antiferromagnetic phase is a sharp central peak at the nearest-neighbor angle $\gamma = \pi$.

For $d = 3$ for the classical Heisenberg spin-glass system, a new phase occurs in the low-temperature quenched-disorder region of the phase diagram, as seen in Figs. 2 and 3, where the spin-glass phase is for the Ising system. The sink of this phase is shown in Figs. 4 and 5. Figure 4 shows, at the sink, the exponentiated nearest-neighbor Hamiltonian $u_{ij}(\gamma) = e^{-\beta\mathcal{H}_{ij}(\vec{s}_i,\vec{s}_j)}$ between sites (i, j) versus the angle γ between the spherical unit vectors $(\vec{s}_i, \vec{s}_j)$. Figure 5 shows, at the sink, the exponentiated nearest-neighbor Hamiltonian $u_{ij}(\gamma)$ versus the angles θ and ϕ between $(\vec{s}_i, \vec{s}_j)$. It is thus seen that the neighboring spins align (nearest-neighbor angle $\gamma = 0$) or antialign ($\gamma = \pi$), globally creating the nematic phase, with a spontaneous alignment axis along which both spin directions occur. All points in the nematic phase flow, under repeated renormalization-group transformations, to this sink which epitomizes the global ordering of this phase.

The spontaneous nematic axis is spontaneously chosen isotropically in the three-dimensional spin space of the model. This characteristic low-temperature high-quenched-disorder phase is also distinctive in its low-temperature penetration into the ferromagnetic and antiferromagnetic phases, in contrast

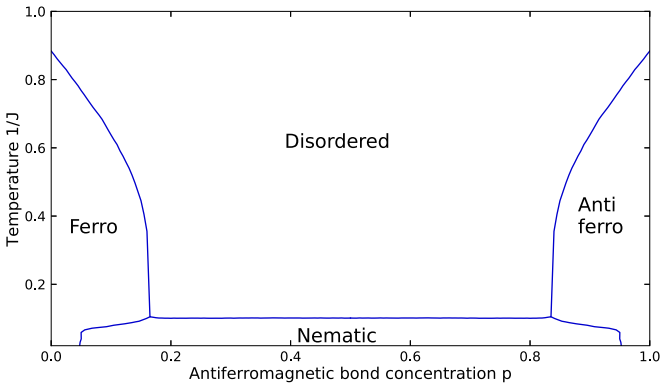

FIG. 2. Calculated phase diagram of the classical Heisenberg spin-glass system in $d = 3$. The phase diagram shows no spin-glass phase, but at low temperatures an extended nematic phase where the spins globally align along a spontaneously chosen axis irrespective of direction. This spontaneous nematic axis is spontaneously chosen isotropically in the three-dimensional spin space of the model. This characteristic low-temperature high-quenched-disorder phase is also distinctive in its low-temperature penetration into the ferromagnetic and antiferromagnetic phases, in contrast to the spin-glass phase.

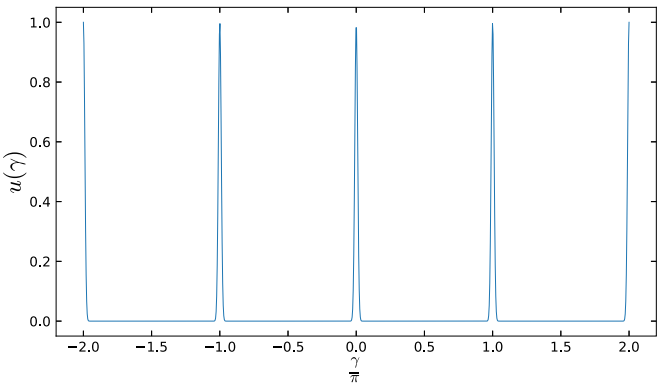

FIG. 4. The fixed-point exponentiated potential $u(\gamma)$ at the renormalization-group sink of the nematic phase. The neighboring spins align (nearest-neighbor angle $\gamma = 0$) or antialign ($\gamma = \pi$), creating the nematic phase with a global spontaneous alignment axis along which both spin directions occur. All points in the nematic phase flow, under repeated renormalization-group transformations, to this sink which epitomizes the ordering of this phase. This potential function, in terms of the nearest-neighbor angle γ, is reconstructed from the Fourier-Legendre coefficients at the renormalization-group sink.

to the spin-glass phase. The nematic phase distinctively penetrates the ferromagnetic and antiferromagnetic phases from higher temperature to its mid-temperature range, where the boundary drops to zero temperature at very low quenched randomness ($p = 0.05, 0.95$). Thus, the nematic phase covers an unusually broad range between $p = 0.05$ and 0.95, where it robustly stretches to finite temperatures.

Thus, it is seen that, in the Heisenberg spin-glass system, at low temperature, this nematic phase extends wider, from $p = 0.05$ to 0.95, as compared with the identically placed spin-glass phase of the Ising spin-glass system which extends between $p = 0.24$ and 0.76 [72]. A similar widening, from $p = 0.24$ to 0.76 to essentially $p = 0$ to 1, is seen [72] in the Ising spin-glass phase, when thermal vacancies are included, making domain flipping more favorable, thus eating into the ferromagnetic (and antiferromagnetic) phases without losing order. A similar mechanism may be in effect in the present

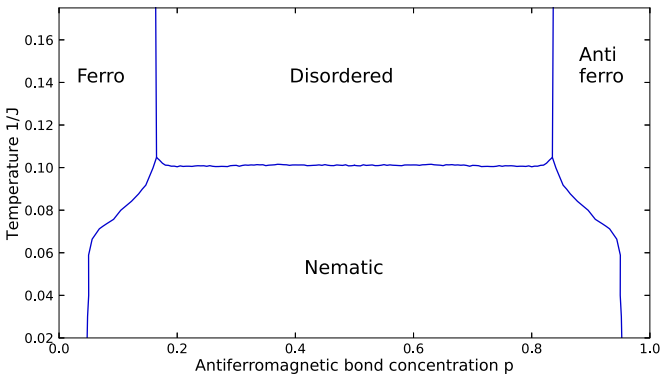

FIG. 3. Low-temperature portion of the calculated phase diagram of the classical Heisenberg spin-glass system in $d = 3$. As more fully seen here, the phase diagram shows no spin-glass phase, but at low temperatures an extended nematic phase where the spins globally align along a spontaneously chosen axis irrespective of direction. The nematic phase distinctively penetrates the ferromagnetic and antiferromagnetic phases to its mid-temperature range, where the boundary drops to zero temperature at very low quenched randomness ($p = 0.05, 0.95$). Thus, the nematic phase covers an unusually broad range between $p = 0.05$ and 0.95, where it robustly stretches to finite temperatures.

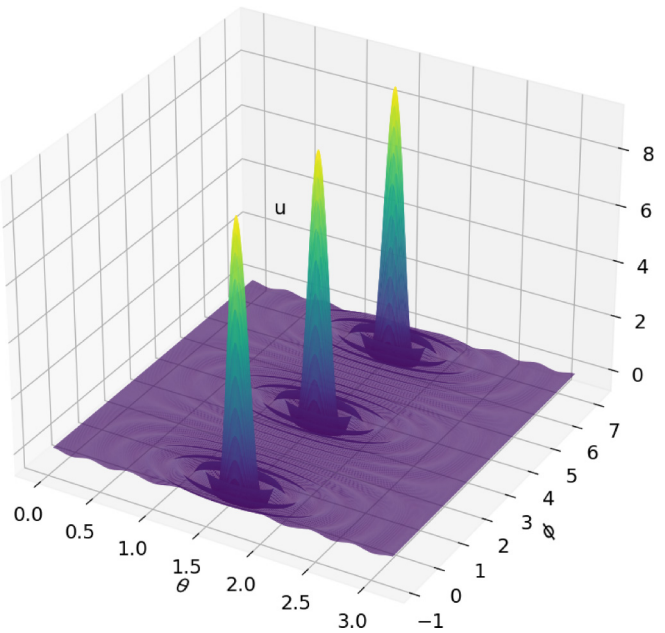

FIG. 5. The fixed-point exponentiated potential $u(\gamma)$ of the sink of the nematic phase of the $d = 3$ classical Heisenberg spin-glass system. This potential function, in terms of the spherical coordinate angles θ and ϕ of one spin with respect to the other, is reconstructed from the Fourier-Legendre coefficients at the sink.

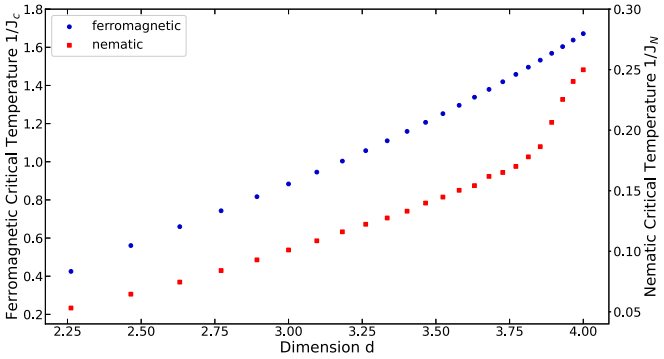

FIG. 6. Calculated transition temperatures for the nematic phase (at $p = 0.5$), squares and right vertical scale, and for the ferromagnetic phase (at $p = 0$), circles and left vertical scale, for 24 different dimensions in $2 < d \leqslant 4$. No nematic (or ferromagnetic [23]) phase occurs in $d = 2$, which is expected.

case, with the continuously varying directions of the Heisenberg spins making domain flipping more favorable.

The calculation is readily extended to other spatial dimensions, including noninteger dimensions, by varying the bond-moving factor $b^{(d-1)} = 3^{(d-1)}$ [11,25,52–55,61,67,69]. The nematic phase of the classical Heisenberg spin-glass system is thus calculated in $d = 2.26,\ 2.46,\ 2.63,\ 2.77,\ 2.89$ dimensions and in dimensions $d \geqslant 3$. Our calculated transition temperatures, for 24 different dimensions in $2 < d \leqslant 4$, are shown in Fig. 6. No nematic (or ferromagnetic [23]) phase occurs in $d = 2$, which is expected. Thus, the lower-critical dimension of the nematic phase is between 2 and 2.26. The standard spin-glass phase does not occur.

VI. CONCLUSION

We have solved the classical Heisenberg spin-glass system by renormalization-group theory. In $d > 2$, in this system with quenched local randomness, a low-temperature phase with global order occurs over an unusually wide disorder range and robustly in the temperature direction, in the form of a spontaneously chosen spin easy axis, irrespective of spin direction. Thus, a nematic phase occurs in the Heisenberg spin system with competing ferromagnetic and antiferromagnetic interactions.

ACKNOWLEDGMENTS

We grateful to E. Can Artun for useful conversations. Support by the TEBIP High Performers Program of the Board of Higher Education of Turkey and by the Academy of Sciences of Turkey (TÜBA) is gratefully acknowledged.

[1] S. F. Edwards and P. W. Anderson, Theory of spin glasses, J. Phys. F **5**, 965 (1975).
[2] G. Toulouse, Theory of frustration effect in spin glasses 1., Commun. Phys. **2**, 115 (1977).
[3] D. Sherrington and S. Kirkpatrick, Solvable Model of a Spin-Glass, Phys. Rev. Lett. **35**, 1792 (1975).
[4] G. Parisi, Infinite Number of Order Parameters for Spin-Glasses, Phys. Rev. Lett. **43**, 1754 (1979).
[5] G. Parisi, Order parameter for spin glasses - Function of the interval 0-1, J. Phys. A **13**, 1101 (1980).
[6] G. Parisi, Magnetic properties of spin glasses in a new mean-field theory, J. Phys. A **13**, 1887 (1980).
[7] J. A. Mydosh, Spin Glasses: Redux: An updated experimental/materials survey, Rep. Prog. Phys. **78**, 052501 (2015).
[8] H. Kawamura and T. Tanigushi, Spin glasses, Handb. Magn. Mater. **24**, 1 (2015).
[9] S. R. McKay, A. N. Berker, and S. Kirkpatrick, Spin-Glass Behavior in Frustrated Ising Models with Chaotic Renormalization-Group Trajectories, Phys. Rev. Lett. **48**, 767 (1982).
[10] S. R. McKay, A. N. Berker, and S. Kirkpatrick, Amorphously packed, frustrated hierarchical models: Chaotic rescaling and spin-glass behavior, J. Appl. Phys. **53**, 7974 (1982).
[11] A. N. Berker and S. R. McKay, Hierarchical models and chaotic spin glasses, J. Stat. Phys. **36**, 787 (1984).
[12] E. C. Artun, I. Keçoğlu, A. Türkoğlu, and A. N. Berker, Multifractal spin-glass chaos projection and interrelation of multicultural music and brain signals, Chaos, Sol. Frac. **167**, 113005 (2023).
[13] H. Kawamura, Spin-chirality decoupling in Heisenberg spin glasses and related systems, J. Magn. Magn. Mater. **310**, 1487 (2007).
[14] H. Kawamura, Dynamical Simulation of Spin-Glass and Chiral-Glass Orderings in Three-Dimensional Heisenberg Spin Glasses, Phys. Rev. Lett. **80**, 5421 (1998).
[15] K. Hukushima and H. Kawamura, Chiral-glass transition and replica symmetry breaking of a three-dimensional Heisenberg spin glass, Phys. Rev. E **61**, R1008(R) (2000).
[16] K. Hukushima and H. Kawamura, Monte Carlo simulations of the phase transition of the three-dimensional isotropic Heisenberg spin glass, Phys. Rev. B **72**, 144416 (2005).
[17] I. Campos, M. Cotallo-Aban, V. Martin-Mayor, S. Perez-Gaviro, and A. Tarancon, Spin-Glass Transition of the Three-Dimensional Heisenberg Spin Glass, Phys. Rev. Lett. **97**, 217204 (2006).
[18] I. A. Campbell and H. Kawamura, Comment on "Spin-Glass Transition of the Three-Dimensional Heisenberg Spin Glass", Phys. Rev. Lett. **99**, 019701 (2007).
[19] L. W. Lee and A. P. Young, Large-scale Monte Carlo simulations of the isotropic three-dimensional Heisenberg spin glass, Phys. Rev. B **76**, 024405 (2007).
[20] L. Fernandez, V. Martin-Mayor, S. Perez-Gaviro, A. Tarancon, and A. P. Young, Phase transition in the three dimensional Heisenberg spin glass: Finite-size scaling analysis, Phys. Rev. B **80**, 024422 (2009).
[21] A. Sharma and A. P. Young, Phase transitions in the one-dimensional long-range diluted Heisenberg spin glass, Phys. Rev. B **83**, 214405 (2011).
[22] T. Ogawa, K. Uematsu, and H. Kawamura, Monte Carlo studies of the spin-chirality decoupling in the three-dimensional Heisenberg spin glass, Phys. Rev. B **101**, 014434 (2020).
[23] E. Tunca and A. N. Berker, Renormalization-group theory of the Heisenberg model in d dimensions, Physica A **608**, 128300 (2022).

[24] A. N. Berker and S. Ostlund, Renormalisation-group calculations of finite systems: Order parameter and specific heat for epitaxial ordering, J. Phys. C **12**, 4961 (1979).
[25] M. Demirtaş, A. Tuncer, and A. N. Berker, Lower-critical spin-glass dimension from 23 sequenced hierarchical models, Phys. Rev. E **92**, 022136 (2015).
[26] R. B. Griffiths and M. Kaufman, Spin systems on hierarchical lattices: Introduction and thermodynamic limit, Phys. Rev. B **26**, 5022 (1982).
[27] M. Kaufman and R. B. Griffiths, Spin systems on hierarchical lattices: 2. Some examples of soluble models, Phys. Rev. B **30**, 244 (1984).
[28] A. A. Migdal, Phase transitions in gauge and spin lattice systems, Zh. Eksp. Teor. Fiz. **69**, 1457 (1975) [Sov. Phys. JETP **42**, 743 (1976)].
[29] L. P. Kadanoff, Notes on Migdal's recursion formulas, Ann. Phys. (NY) **100**, 359 (1976).
[30] P. J. Flory, *Principles of Polymer Chemistry* (Cornell University Press, Ithaca, NY, 1986).
[31] M. Kaufman, Entropy driven phase transition in polymer gels: Mean field theory, Entropy **20**, 501 (2018).
[32] P. Lloyd and J. Oglesby, Analytic approximations for disordered systems, J. Phys. C: Solid St. Phys. **9**, 4383 (1976).
[33] R. H. Kraichnan, Dynamics of nonlinear stochastic systems, J. Math. Phys. **2**, 124 (1961).
[34] K. Jiang, J. Qiao, and Y. Lan, Chaotic renormalization flow in the Potts model induced by long-range competition, Phys. Rev. E **103**, 062117 (2021).
[35] G. Mograby, M. Derevyagin, G. V. Dunne, and A. Teplyaev, Spectra of perfect state transfer Hamiltonians on fractal-like graphs, J. Phys. A **54**, 125301 (2021).
[36] I. Chio and R. K. W. Roeder, Chromatic zeros on hierarchical lattices and equidistribution on parameter space, Ann. Inst. Henri Poincaré D **8**, 491 (2021).
[37] B. Steinhurst and A. Teplyaev, Spectral analysis on Barlow and Evans' projective limit fractals, J. Spectr. Theory **11**, 91 (2021).
[38] A. V. Myshlyavtsev, M. D. Myshlyavtseva, and S. S. Akimenko, Classical lattice models with single-node interactions on hierarchical lattices: The two-layer Ising model, Physica A **558**, 124919 (2020).
[39] M. Derevyagin, G. V. Dunne, G. Mograby, and A. Teplyaev, Perfect quantum state transfer on diamond fractal graphs, Quantum Inf. Process. **19**, 328 (2020).
[40] S.-C. Chang, R. K. W. Roeder, and R. Shrock, q-plane zeros of the Potts partition function on diamond hierarchical graphs, J. Math. Phys. **61**, 073301 (2020).
[41] C. Monthus, Real-space renormalization for disordered systems at the level of large deviations, J. Stat. Mech.: Theory Exp. (2020), 013301.
[42] O. S. Sarıyer, Two-dimensional quantum-spin-1/2 XXZ magnet in zero magnetic field: Global Thermodynamics from renormalisation group theory, Philos. Mag. **99**, 1787 (2019).
[43] P. A. Ruiz, Explicit formulas for heat kernels on diamond fractals, Commun. Math. Phys. **364**, 1305 (2018).
[44] M. J. G. Rocha-Neto, G. Camelo-Neto, E. Nogueira, Jr., and S. Coutinho, The Blume–Capel model on hierarchical lattices: Exact local properties, Physica A **494**, 559 (2018).
[45] F. Ma, J. Su, Y. X. Hao, B. Yao, and G. G. Yan, A class of vertex–edge-growth small-world network models having scale-free, self-similar and hierarchical characters, Physica A **492**, 1194 (2018).
[46] S. Boettcher and S. Li, Analysis of coined quantum walks with renormalization, Phys. Rev. A **97**, 012309 (2018).
[47] A. N. Berker, S. Ostlund, and F. A. Putnam, Renormalization-group treatment of a Potts lattice gas for krypton adsorbed onto graphite, Phys. Rev. B **17**, 3650 (1978).
[48] S. Ostlund and A. N. Berker, Multicritical Phase Diagram of Gases Adsorbed on Graphite: Temperature Variation and Finite Size Effects, Phys. Rev. Lett. **42**, 843 (1979).
[49] M. Hinczewski and A. N. Berker, Finite-temperature phase diagram of nonmagnetic impurities in high-temperature superconductors using a $d = 3tJ$ model with quenched disorder, Phys. Rev. B **78**, 064507 (2008).
[50] J. V. José, L. P. Kadanoff, S. Kirkpatrick, and D. R. Nelson, Renormalization, vortices, and symmetry-breaking perturbations in two-dimensional planar model, Phys. Rev. B **16**, 1217 (1977).
[51] A. N. Berker and D. R. Nelson, Superfluidity and phase separation in helium films, Phys. Rev. B **19**, 2488 (1979).
[52] H. Y. Devre and A. N. Berker, First-order to second-order phase transition changeover and latent heats of q-state Potts models in $d = 2, 3$ from a simple Migdal-Kadanoff adaptation, Phys. Rev. E **105**, 054124 (2022).
[53] M. S. Cao and J. Machta, Migdal-Kadanoff study of the random-field Ising model, Phys. Rev. B **48**, 3177 (1993).
[54] A. Falicov, A. N. Berker, and S. R. McKay, Renormalization-group theory of the random-field Ising model in three dimensions, Phys. Rev. B **51**, 8266 (1995).
[55] K. Akın and A. N. Berker, Lower critical dimension of the random-field XY model and the zero-temperature critical line, Phys. Rev. E **106**, 014151 (2022).
[56] S. Franz, G. Parisi, and M. A. Virasoro, Interfaces and lower critical dimension in a spin-glass Model, J. Phys. I **4**, 1657 (1994).
[57] C. Amoruso, E. Marinari, O. C. Martin, and A. Pagnani, Scalings of Domain Wall Energies in Two Dimensional Ising Spin Glasses, Phys. Rev. Lett. **91**, 087201 (2003).
[58] J.-P. Bouchaud, F. Krzakala, and O. C. Martin, Energy exponents and corrections to scaling in Ising spin glasses, Phys. Rev. B **68**, 224404 (2003).
[59] S. Boettcher, Stiffness of the Edwards-Anderson Model in all Dimensions, Phys. Rev. Lett. **95**, 197205 (2005).
[60] A. Maiorano and G. Parisi, Support for the value 5/2 for the spin glass lower critical dimension at zero magnetic field, Proc. Natl. Acad. Sci. U.S.A. **115**, 5129 (2018).
[61] B. Atalay and A. N. Berker, A lower lower-critical spin-glass dimension from quenched mixed-spatial-dimensional spin glasses, Phys. Rev. E **98**, 042125 (2018).
[62] M. Aizenman and J. Wehr, Rounding of First-Order Phase Transitions in Systems with Quenched Disorder, Phys. Rev. Lett. **62**, 2503 (1989).
[63] M. Aizenman and J. Wehr, Erratum: Rounding of First-Order Phase Transitions in Systems with Quenched Disorder, Phys. Rev. Lett. **64**, 1311(E) (1990).
[64] K. Hui and A. N. Berker, Random-Field Mechanism in Random-Bond Multicritical Systems, Phys. Rev. Lett. **62**, 2507 (1989).

[65] K. Hui and A. N. Berker, Erratum: Random-Field Mechanism in Random-Bond Multicritical Systems, Phys. Rev. Lett. **63**, 2433(E) (1989).

[66] E. Ilker and A. N. Berker, High q-state clock spin glasses in three dimensions and the Lyapunov exponents of chaotic phases and chaotic phase boundaries, Phys. Rev. E **87**, 032124 (2013).

[67] E. Ilker and A. N. Berker, Overfrustrated and underfrustrated spin glasses in $d = 3$ and 2: Evolution of phase diagrams and chaos including spin-glass order in $d = 2$, Phys. Rev. E **89**, 042139 (2014).

[68] E. Ilker and A. N. Berker, Odd q-state clock spin-glass models in three dimensions, asymmetric phase diagrams, and multiple algebraically ordered phases, Phys. Rev. E **90**, 062112 (2014).

[69] T. Çağlar and A. N. Berker, Chiral Potts spin glass in $d = 2$ and 3 dimensions, Phys. Rev. E **94**, 032121 (2016).

[70] T. Çağlar and A. N. Berker, Devil's staircase continuum in the chiral clock spin glass with competing ferromagnetic-antiferromagnetic and left-right chiral interactions, Phys. Rev. E **95**, 042125 (2017).

[71] T. Çağlar and A. N. Berker, Phase transitions between different spin-glass phases and between different chaoses in quenched random chiral systems, Phys. Rev. E **96**, 032103 (2017).

[72] G. Gülpınar and A. N. Berker, Quenched-vacancy induced spin-glass order, Phys. Rev. E **79**, 021110 (2009).